ML-7 treatment but not the Y-27632 treatment significantly suppressed the speed of cell motility, measured as 5-min displacements, in analysis of variance tests versus the control [control: 1.32 ± 0.08 μm (mean $\pm$ SEM), $n = 41$ cells; ML-7 treatment: 1.11 ± 0.07 μm, $n = 42$ cells, $P < 0.05$; Y-27632 treatment: 1.49 ± 0.07 μm, $n = 41$ cells, not significant] (5). Finally, treatment with 500 nM nocodazole for 30 min (Fig. 4, M to O) led to the complete disruption of cytoplasmic microtubules and, although ruffling activity was changed in character (Fig. 4N), there were indications that labeled actin was still rapidly recruited to the leading edge (Fig. 4O).

In summary, we found that actin polymerized during protrusion of the leading edge can be recruited within 2 to 3 s from a region that extends up to 15 μm behind the edge. This process is too rapid to be explained by diffusion of G-actin and must involve some form of active transport. It requires G-actin, adenosine triphosphate, and active protrusion but not intact microtubules. The effects of MLCK inhibition indicate that myosin function is required for rapid actin transport, although not for ruffling. The similar effects of ROCK inhibition further suggest that the required myosin is activated by Rho and is probably nonmuscle myosin II.

We conclude that G-actin is not carried rapidly to the leading edge by microtubule-based motors or by motor proteins of the myosin superfamily. Myosin II is unlikely to transport actin directly, but it is needed for contraction of the cell body. This could generate a pressure gradient leading to a hydrodynamic flow that carries G-actin with it. The flow would be directed toward sites of reduced pressure that may occur where the cell margin is expanding rapidly. Such rapid expansion might occur passively at sites of cortical weakness or actively where polymerizing actin is pushing the membrane outward (1). Pressure-driven flow through gels can result in channeling, and there is some evidence for this in the figures. Retraction of the cell margin may occur by Rho-dependent contraction (8), in which case the mechanism we propose could account for a reported positive correlation between rates of protrusion and retraction (9). Rapid actin transport is not required for cell locomotion or for ruffling, which is thought to be regulated by Rac (10), but it may determine sites of protrusion and thus participate in signal-mediated cell polarity and directed locomotion. Our view is that hydrodynamic flow supplies actin from sites of high depolymerization to sites of rapid protrusion where diffusion alone is inadequate.

References and Notes
1. T. D. Pollard, L. Blanchoin, R. D. Mullins, *Annu. Rev. Biophys. Biomol. Struct.* **29**, 545 (2000).
2. D. Pantaloni, C. Le Clainche, M. F. Carlier, *Science* **292**, 1502 (2001).
3. N. Watanabe, T. J. Mitchison, *Science* **295**, 1083 (2002).
4. G. A. Dunn, I. M. Dobbie, J. Monypenny, M. R. Holt, D. Zicha, *J. Microsc.* **205**, 109 (2002).
5. Materials and methods are available as supporting material on *Science* Online.
6. J. L. McGrath, Y. Tardy, C. F. Dewey Jr., J. J. Meister, J. H. Hartwig, *Biophys. J.* **75**, 2070 (1998).
7. B. P. Olveczky, A. S. Verkman, *Biophys. J.* **74**, 2722 (1998).
8. R. A. Worthylake, S. Lemoine, J. M. Watson, K. Burridge, *J. Cell Biol.* **154**, 147 (2001).
9. G. A. Dunn, D. Zicha, *J. Cell Sci.* **108**, 1239 (1995).
10. A. J. Ridley, H. F. Paterson, C. L. Johnston, D. Diekmann, A. Hall, *Cell* **70**, 401 (1992).
11. Supported by Medical Research Council (UK) Programme grant G0300046-64953 (G.A.D.). We thank P. Jordan and P. Fraylich for technical assistance.

Forces for Morphogenesis Investigated with Laser Microsurgery and Quantitative Modeling

M. Shane Hutson,[1] Yoichiro Tokutake,[1] Ming-Shien Chang,[1]* James W. Bloor,[2]† Stephanos Venakides,[3] Daniel P. Kiehart,[2]‡§ Glenn S. Edwards[1]‡§

We investigated the forces that connect the genetic program of development to morphogenesis in *Drosophila*. We focused on dorsal closure, a powerful model system for development and wound healing. We found that the bulk of progress toward closure is driven by contractility in supracellular "purse strings" and in the amnioserosa, whereas adhesion-mediated zipping coordinates the forces produced by the purse strings and is essential only for the end stages. We applied quantitative modeling to show that these forces, generated in distinct cells, are coordinated in space and synchronized in time. Modeling of wild-type and mutant phenotypes is predictive; although closure in *myospheroid* mutants ultimately fails when the cell sheets rip themselves apart, our analysis indicates that β_{PS} integrin has an earlier, important role in zipping.

Dorsal closure, an essential stage of *Drosophila* embryogenesis, has been extensively studied (*1–7*). However, an understanding of the cellular and molecular mechanisms that generate force and drive tissue dynamics in this process has been elusive. The quantitative and predictive capabilities of physical modeling (*8–11*) now offer a powerful set of tools to address this problem. The dynamics of dorsal closure can be visualized in living embryos with the use of green fluorescent protein (GFP) transgenes that label the actin cytoskeleton (Fig. 1A) (*12–14*). In the early stages of closure, the dorsal surface of the embryo is covered by large, flat polygonal cells of the amnioserosa. The rest of the embryo is covered by cells of the lateral and ventral epidermis which are smaller and cuboidal to columnar in shape. The visible area of the amnioserosa is shaped roughly like a human eye, with a wide central section that tapers to canthi, the corners of the eye (Fig. 1A). A single row of amnioserosa cells is tucked under the lateral epidermis throughout closure (*12*). Where these cell sheets overlap, the most dorsal row of lateral epidermis cells comprises a third distinct tissue known as the leading edge of the lateral epidermis (*12, 15, 16*). The cells of the leading edge on each flank of the embryo contain an actin-rich supracellular "purse string" (*4, 6, 12*). In addition, these cells extend dynamic fingerlike filopodia, ~10 μm in length (*13*). At the canthi, pairs of these filopodia can span the gap between opposing leading edges. As dorsal closure progresses, each structure changes (*6, 12*): Cells of the lateral epidermis stretch toward the dorsal midline, the supracellular purse strings contract along their length, and the cells of the amnioserosa actively and asymmetrically change shape as their apical surfaces contract. Concomitant with these movements, the two flanks of the lateral epidermis are zipped together as filopodia and lamellipodia from opposing leading edges interdigitate to form a seam (*13, 17, 18*). The bulk of closure requires ~2 to 3 hours.

Dorsal closure has previously been examined through mechanical, laser, and genetic perturbations. Laser-ablation experiments

[1]Department of Physics and Free Electron Laser Laboratory, [2]Department of Biology, [3]Department of Mathematics, Duke University, Durham, NC 27708, USA.

*Present address: School of Physics, Georgia Institute of Technology, Atlanta, GA 30332, USA.
†Present address: Research School of Biosciences, University of Kent, Canterbury, Kent CT2 7NJ, UK.
‡These authors contributed equally to this work.
§To whom correspondence should be addressed. E-mail: dkiehart@duke.edu (D.P.K.); edwards@fel.duke.edu (G.S.E.)

have shown that all the tissues involved are under tension (*12*). Thus, the lateral epidermis is stretched by contractile forces generated both within individual cells of the amnioserosa and within the purse strings. When laser ablation locally eliminates tension in either the amnioserosa or purse strings, dorsal closure proceeds. In contrast, when both are ablated, closure fails (*12*). Closure may also fail following genetic perturbations (*1–3*, *6*, *13*, *19–21*). These experiments have highlighted the relevance of both contractile actomyosin assemblies and adhesive filopodial contacts to dorsal closure, but have not revealed their relative importance or their possible interaction.

Here, we investigated dorsal closure by dissecting the forces and processes involved through laser microsurgery and quantitative modeling. We focused on the middle to late stages of dorsal closure when the entire leading edge can be imaged in a single focal plane. We optimized our laser microbeam to near diffraction-limited performance, added computer-steering, and used automated image processing routines to analyze the dynamic geometry of native and perturbed embryos (*14*). Time-lapse videos of the embryos reported in Fig. 1 are available online (movies S1 to S5). From these experiments, we deduced the relative magnitudes of the contributing forces resulting from the lateral epidermis, amnioserosa, and purse strings. We constructed a quantitative model of dorsal closure to describe the dynamic geometry of native and perturbed embryos. By applying this model to a β_{PS} integrin mutant, we quantified the mutant phenotype and specified the force-generating process(es) to which the protein contributes.
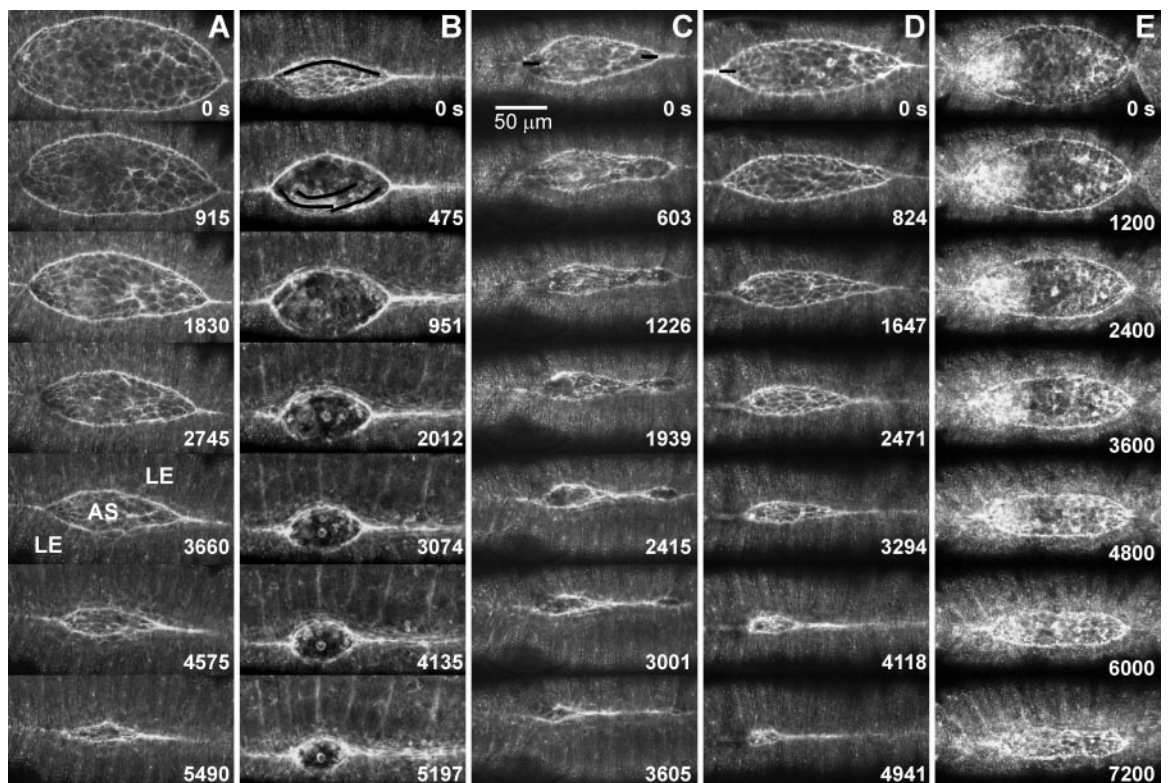
To evaluate the contribution of the amnioserosa to dorsal closure, we removed the exposed amnioserosa with laser incisions (*14*). After this dissection, the curvature of the purse strings and the area they enclose increased by more than a factor of 2 (Fig. 1B). In Fig. 2, we track the area enclosed by the purse strings as a function of time, $A(t)$, for native and laser-dissected embryos. Because we observe a ~20% variability in native closure times from $A \sim 6000 \ \mu m^2$, we have included both fast and slow extremes. After the removal of the amnioserosa, the closure time is ~400% of that for native embryos. Additional observations confirm a central role in dorsal closure for contractile forces in the amnioserosa.

To evaluate the contribution of zipping, we laser-inhibited this process at one or both canthi (*14*). When zipping was inhibited at both canthi, the two flanks of lateral epidermis continued their progress toward the dorsal midline and eventually zipping resumed from new interior foci (Fig. 1C). As closure continued, the interior seam then expanded toward both ends of the embryo. When laser microsurgery halted zipping at one canthus, zipping proceeded from the other, where the rate can actually increase (Fig. 1D). Surprisingly, laser inhibition of zipping introduced only small delays in closure (one canthus, 9 to 32% longer; both canthi, 17 to 40% longer). These delays lie just outside the variability observed for native embryos (Fig. 2) and may be caused by damage to the underlying amnioserosa. These experiments demonstrate that there are mechanisms in place that can bring opposing flanks of the lateral epidermis into close proximity even in the absence of zipping. Preliminary experiments indicate that the amnioserosa is critical for this process; when we remove the amnioserosa and inhibit zipping, closure fails.

When zipping was inhibited at both canthi, sustained indentations of the leading edge later became new foci from which zipping resumed. In the embryo shown in Fig. 1C, such indentations (i.e., regions concave to the dorsal midline) appeared ~1400 s after the initial incision, when the leading edges moved to within 10 to 15 μm of one another. In contrast, transient changes in concavity occurred after each laser incision as a result of leading edge retraction near each cut (Fig. 1C, first three panels). Two processes may contribute to the formation of sustained indentations. The indentations could be the consequence of a wound-healing response that results in an increased localized contraction of the amnioserosa. Alternatively, filopodia may mediate their formation, given that a previous report has found that their reach, ~10 μm (*13*), is consistent with the distance between the leading edges when these indentations were first observed. It is unlikely that

Fig. 1. Confocal fluorescent images of native and perturbed dorsal closure (AS, amnioserosa; LE, lateral epidermis). (**A**) Native embryos; (**B**) a series of four cuts to completely dissect the exposed amnioserosa; (**C**) laser inhibition of zipping at both canthi; (**D**) laser inhibition of zipping at one canthus; and (**E**) *myospheroid* mutant embryos. Black lines locate laser incisions; elapsed time starts at first lasing. The scale bar applies to all images. Posterior is to the left.

filopodia mediate this entire process because these sites were initially separated by 24 to 35 μm. Nevertheless, the establishment of new foci illustrates the importance of zipping during the end stages of closure.

To understand dorsal closure quantitatively, we next concentrated on the force balance at the leading edge. As shown in Fig. 3A, we treated the purse string as a cable under tension, $\mathbf{T}$, that is subjected to a force per unit length from both the lateral epidermis, $\sigma_{\mathbf{LE}}$, and the amnioserosa, $\sigma_{\mathbf{AS}}$. The segment is also subject to a viscous drag proportional to its velocity, $\mathbf{v}$. Under the conditions of low Reynolds number (22), where viscous forces far outweigh inertia, application of Newton's second law to a small segment of the leading edge at the symmetry postion yields

$$\sigma_{\text{LE}} - \sigma_{\text{AS}} - T\kappa = b \, dh/dt \qquad (1)$$

(14), where h is the distance from the dorsal midline to the leading edge along the symmetry axis, κ is the curvature of the purse string, and $b \, dh/dt$ is the viscous drag per unit length.
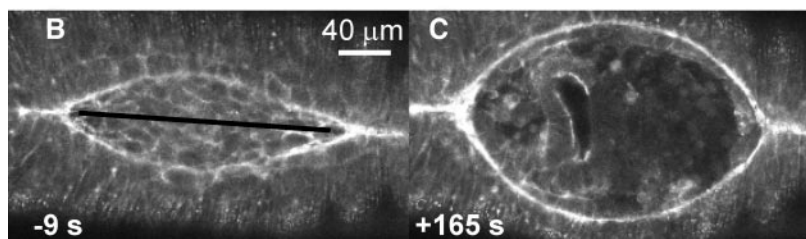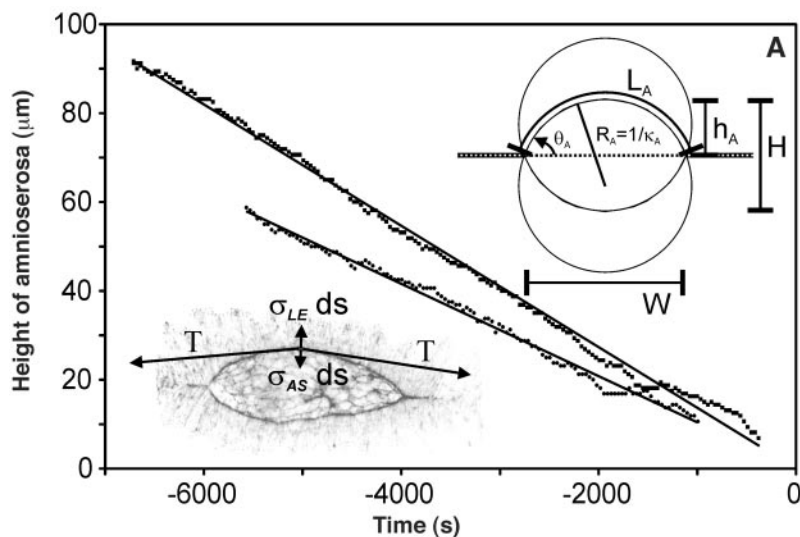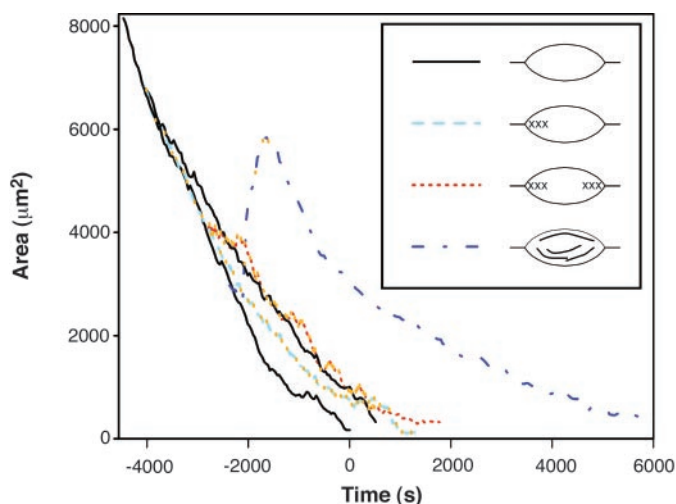
The observation of native embryos reveals that each $h(t)$, and their sum $H(t)$ (Fig. 3A), decrease linearly with time ($dH/dt = -12.0 \pm 1.5$ nm/s, $N = 5$). As an immediate consequence of this striking linear behavior, the sum of the applied forces on the left side of Eq. 1 remains constant throughout closure.

To quantify the ratio of these forces, we performed mechanical-jump experiments in which the force due to the amnioserosa is rapidly (<10 s) removed with a linear incision from canthus to canthus (Fig. 3, B and C). The leading edges then retract from one another at an initial rate of 940 ± 270 nm/s. The force removed by an incision is proportional to the resulting change in velocity, provided that the coefficient b is constant. Neglecting the velocity dependence of b introduces an error that is small relative to the experimental error and biological variability (14). Thus, the force of the amnioserosa is greater than the net applied force by a factor of at least ~80 (i.e., 940/12).

After the incision, the leading edges retract for several minutes until they reach a turning point, where the applied forces are in balance, and closure resumes. The contributions of T and σ_{AS} to the motion of the leading edge are obtained by comparing Eq. 1 at the turning point with Eq. 1 before the incision (14). By performing mechanical jumps on a number of embryos at different stages, we determined the stage-dependence of $T\kappa/\sigma_{\text{AS}}$ (fig. S2A). Through most of closure, the forces produced by the amnioserosa and purse strings make comparable contributions to the motion of the leading edge along the y axis. During the middle to late stages, $A < 8000$ μm², the average ratio is $T\kappa/\sigma_{\text{AS}} = 0.7 \pm 0.3$. Because the net applied force is smaller than σ_{AS} by a factor of ~80, it can be shown that the relative magnitudes of the force contributions toward closure, $\sigma_{\text{LE}}:\sigma_{\text{AS}}:T\kappa:bv$, are bracketed between the ratios ~120:80:40:1 and ~160:80:80:1. Similarly, the ratio $T:\sigma_{\text{AS}}\Delta s_{\text{AS}}:\sigma_{\text{LE}}\Delta s_{\text{LE}}$ decreases from ~36:2:1 to ~8:2:1 (fig. S2B). Although T is the largest force from this perspective, its contribution toward closure, $T\kappa$, is relatively small because of the moderate curvature of the purse string (1/κ of 50 to 250 μm) when compared to cellular dimensions ($\Delta s_{\text{AS}} = 10$ μm, $\Delta s_{\text{LE}} = 3$ μm).

Next, to describe zipping at the two canthi, we were able to model the changing geometry of dorsal closure without addressing the specific forces. We view the purse strings as two intersecting circular arcs with similar, but not necessarily identical, radii. As shown in Fig. 4, this approximates the overall shape of the leading edge as it approaches closure. Using the subscripts A and

Fig. 2. Time courses of the area enclosed by the purse strings: fast and slow extremes of native closure (solid curves); repetitive laser incisions to inhibit zipping at one canthus (dashed curve); repetitive laser incisions to inhibit zipping at both canthi (dotted curve); and dissection of the exposed amnioserosa (dot-dashed curve). Orange dots indicate times of laser incisions. The inset shows diagrams of the incisions corresponding to each curve. Origins were chosen so that the curves overlap at early times.

Fig. 3. Forces in dorsal closure. (**A**) The upper inset defines the geometric parameters used to describe dorsal closure. The lower inset is a schematic force diagram for a segment (*ds*) of the leading edge at the symmetry point. For both fast (top curve) and slow (bottom curve) extremes of native dorsal closure, the height of the amnioserosa, *H(t)*, decreases linearly. (**B**) An image of dorsal closure prior to a mechanical jump experiment, and (**C**) at the turning point (see text).

B to denote the two purse strings, a full description of the time-dependent geometry requires only three variables: the width of the amnioserosa, W; and any pair $L_{A/B}$, $h_{A/B}$, $\theta_{A/B}$, or $R_{A/B}$. Given the previous discussion, the natural choice is the pair $h_{A/B}$. An empirically derived rate equation (14) describes the zipping rate, dW/dt, that incorporates the leading edges into the seam:

$$\frac{dW}{dt} =$$

$$\frac{-k_z}{\tan(\theta_A/2) + \tan(\theta_B/2)} = \frac{-k_zW}{2H} \quad (2)$$

where $H = h_A + h_B$ and k_z is a rate constant. dW/dt is only dependent upon the purse-string geometry through the angles at the canthi, $\theta_{A/B}(t)$. The rightmost term in Eq. 2 arises by expressing $\theta_{A/B}$ in terms of W and $h_{A/B}$. Equation 2 has the general and biologically reasonable property that dW/dt quickens as $\theta_{A/B}$ becomes more acute. Moreover, when zipping is inhibited at one canthus, Eq. 2 provides a rationale for the increased zipping rate observed at the other (Fig. 1D).

We first applied this model to situations in which dH/dt is constant with $V = v_A + v_B$, such as native closure. Using the linear solution for $H(t)$ to integrate Eq. 2 yields an explicit analytic solution for $W(t)$ that provides an excellent fit to native closure (Fig. 4, A and B):

$$W(t) = W(0)\left[\frac{H(t)}{H(0)}\right]^{k_z/2V} =$$

$$W(0)\left[1 - \frac{Vt}{H(0)}\right]^{k_z/2V} \quad (3)$$

In our data and in the fitted solution, the rate of zipping increases slowly with time. This treatment also applies to any period of perturbed closure for which dH/dt is constant (Fig. 4, C and D). Nonlinear regression is used to find the rate constants k_z and V that characterize dorsal closure under a variety of conditions (table S1).
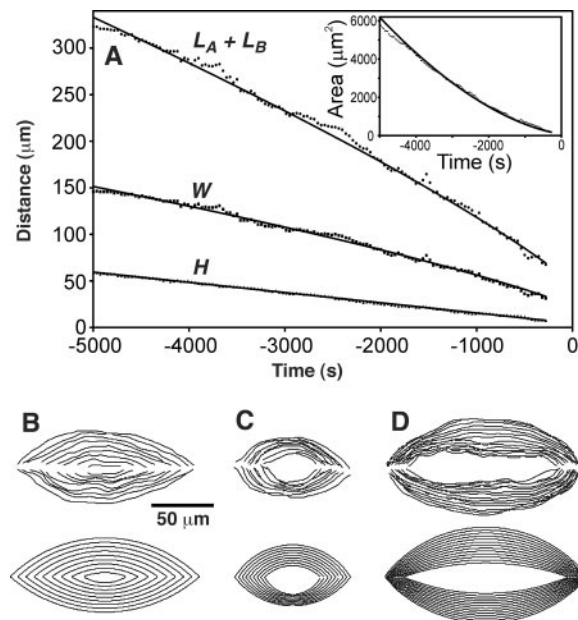
Purse-string contraction and zipping are processes that directly reduce the length of the leading edge. We gained additional insight by assessing how these length changes are translated into fractional contributions to the velocity of closure, dH/dt, under the conditions of arc geometry inherent in the data and model. The fractional contribution of zipping to dH/dt is $f_z = k_z/4V$ (14), with the remainder of dH/dt attributable to contraction ($f_c = 1 - f_z$). We find that $f_z \approx 1/3$ in native closure, consistent with the 17 to 40% delay shown in Fig. 2 for laser inhibition of zipping. When a sequence of laser incisions compromises zipping (Fig. 1C), we find that $f_z \approx 1/12$. We expect $f_z = 0$ for complete inhibition. When the amnioserosa is removed by laser microsurgery (Fig. 1B), k_z and V decrease to 66% and 46% of the native rates, respectively, resulting in an increase of f_z to nearly ½. Thus, these laser protocols perturb the rate constants in a systematic manner (table S1), providing a theoretical framework to quantify genetic perturbations of dorsal closure.

We have applied this model to *myospheroid* embryos (Figs. 1E and 4D) that have defects in β_{PS} integrin (23), a cell surface receptor that mediates both cellular adhesion and bidirectional signaling between the cytoplasmic and extracellular environments. Ultimately, both the amnioserosa and lateral epidermis rip themselves apart and the embryos fail to complete closure. Until then, dH/dt is constant at ~60% of the wild-type velocity. Fitting the dynamic geometry to our model shows that the rate constant for zipping decreases to less than 20% of the wild-type rate constant. Thus, before outright failure, a key element of the *myospheroid* phenotype is a strong deficiency in zipping (f_z drops to ~1/10). This result contradicts previous suggestions that β_{PS} integrin contributes by anchoring leading-edge cells to the underlying amnioserosa (1). In native embryos, purse-string contraction and zipping are coordinated for dorsal closure to proceed. As observed in *myospheroid*, deficient zipping in the presence of continued purse-string contraction leads to decreases in κ as closure progresses. Thus, T is less effectively applied along the direction of motion. Compensatory changes in the forces, either a decrease in $\sigma_{LE} - \sigma_{AS}$ or an increase in T, allow closure to progress in these embryos until the curvature has decreased substantially (Figs. 1E and 4D). Scores of mutations lead to failures in dorsal closure (1–3). This model promises to quantify their phenotypes and elucidate the molecular basis of morphogenesis.

Dorsal closure is characterized by a set of cellular processes that produce force: contractile forces caused by purse strings in the leading edge of the lateral epidermis; contractile forces caused by the cortical actin networks of individual amnioserosa cells; resistance caused by stretching of the lateral epidermis; and zipping at the canthi. We quantified the contributions of each from three different perspectives. First, in terms of the forces applied to the leading edge in native closure, the magnitude of the vector sum of the applied forces at the symmetry point is a small fraction of the magnitude of any single applied force, and it is remarkably constant, i.e., $\sigma_{LE}:\sigma_{AS}:T\kappa:bv$ lies between ~120:80:40:1 and ~160:80:80:1. Second, laser and genetic perturbations confirm that contractile forces from the amnioserosa and purse string are the dominant contributors to the motion of the leading edges before the end stages of closure, i.e., zipping is not strictly required for closure to progress. Our data suggest that when one process is defective, others can compensate, highlighting the redundancy and resiliency of dorsal closure. Third, in terms of a rate process description of native closure, contraction contributes two-thirds and zipping one-third to the velocity of the leading edges. Although zipping does not contribute a force for the movement of the leading edge at sites that are far removed from the canthi, the adhesive contacts provide an anchor for T and the rate of zipping influences κ. Further investigation of the structures that produce force at the canthi should allow the connection of the force and rate-process perspectives. This approach promises high-resolution interrogation of tissue dynamics in morphogenesis and wound healing throughout phylogeny. We anticipate that the application of these techniques

Fig. 4. Empirical rate equations model dorsal closure. Model (solid lines) and experimental observations for (**A**) native closure: total perimeter, $L_A + L_B$; width, W; total height, H; and (inset) area, A. Comparison of the observed (upper) and modeled (lower) contours of the purse strings for dorsal closure (**B**) in native embryos, (**C**) after laser dissection of the amnioserosa, and (**D**) in *myospheroid* mutant embryos. The time between successive contours is 600 s. The scale bar applies to all contours.

to transgenic and mutant animals will further reveal the molecular basis of tissue dynamics during development.

References and Notes

1. A. Jacinto, S. Woolner, P. Martin, *Dev. Cell* **3**, 9 (2002).
2. N. Harden, *Differentiation* **70**, 181 (2002).
3. F. Agnes, S. Noselli, *C. R. Acad. Sci. Paris Sci. Vie* **322**, 5 (1999).
4. D. P. Kiehart, *Curr. Biol.* **9**, R602 (1999).
5. J. A. Campos-Ortega, V. Hartenstein, *The Embryonic Development of* Drosophila melanogaster (Springer-Verlag, New York, 1985).
6. P. E. Young, A. M. Richman, A. S. Ketchum, D. P. Kiehart, *Genes Dev.* **7**, 29 (1993).
7. A. Martinez-Arias, in *The Development of* Drosophila melanogaster, A. Martinez-Arias, M. Bates, Eds. (Cold Spring Harbor Laboratory Press, Cold Spring Harbor, NY, 1993), pp. 517–607.
8. H. Meinhardt, S. Roth, *Nature* **419**, 261 (2002).
9. A. Eldar *et al.*, *Nature* **419**, 304 (2002).
10. H. H. Chen, G. W. Brodland, *J. Biomech. Eng.* **122**, 394 (2000).
11. L. A. Davidson, G. F. Oster, R. E. Keller, M. A. Koehl, *Dev. Biol.* **209**, 221 (1999).
12. D. P. Kiehart, C. G. Galbraith, K. A. Edwards, W. L. Rickoll, R. A. Montague, *J. Cell Biol.* **149**, 471 (2000).
13. A. Jacinto *et al.*, *Curr. Biol.* **10**, 1420 (2000).
14. Materials and methods are available as supporting material on *Science* Online.
15. B. E. Stronach, N. Perrimon, *Development* **128**, 2905 (2001).
16. V. E. Foe, *Development* **107**, 1 (1989).
17. J. W. Bloor, D. P. Kiehart, *Development* **129**, 3173 (2002).
18. C. R. Magie, M. R. Meyer, M. S. Gorsuch, S. M. Parkhurst, *Development* **126**, 5353 (1999).
19. B. H. Reed, R. Wilk, H. D. Lipshitz, *Curr. Biol.* **11**, 1098 (2001).
20. N. Harden *et al.*, *J. Cell Sci.* **115**, 2119 (2002).
21. A. Jacinto *et al.*, *Curr. Biol.* **12**, 1245 (2002).
22. E. M. Purcell, *Am. J. Phys.* **45**, 3 (1977).
23. A. J. MacKrell, B. Blumberg, S. R. Haynes, J. H. Fessler, *Proc. Natl. Acad. Sci. U.S.A.* **85**, 2633 (1988).
24. We thank R. Fehon, T. Kephart, D. McClay, and members of the Kiehart laboratory for critical reading of the manuscript; A. Boury and R. Montague for fly husbandry; and F. Malik and J. Sabry for suggesting the term canthus. Supported by the Department of Defense/Air Force Office of Scientific Research Medical Free Electron Laser (F49620-00-1-0370) and by the NIH (GM33830 and GM61240).